Inorganic Chemistry

Article

pubs.acs.org/IC

First Row Transition Metal(II) Thiocyanate Complexes, and Formation of 1-, 2-, and 3-Dimensional Extended Network Structures of $M(NCS)_2(Solvent)_2$ (M = Cr, Mn, Co) Composition

Endrit Shurdha,[†,∥] Curtis E. Moore,[§] Arnold L. Rheingold,[§] Saul H. Lapidus,[‡,⊥] Peter W. Stephens,[‡] Atta M. Arif,[†] and Joel S. Miller*[,†]

[†]Department of Chemistry, University of Utah, Salt Lake City, Utah 84112-0850, United States

[‡]Department of Physics and Astronomy, Stony Brook University, Stony Brook, New York 11794, United States

[§]Department of Chemistry, University of California, San Diego, La Jolla, California 92093-0358, United States

Supporting Information

ABSTRACT: The reaction of first row transition M^{II} ions with KSCN in various solvents form tetrahedral $(NMe_4)_2[M^{II}(NCS)_4]$ (M = Fe, Co), octahedral *trans*-$M^{II}(NCS)_2(Sol)_4$ (M = Fe, V, Ni; Sol = MeCN, THF), and $K_4[M^{II}(NCS)_6]$ (M = V, Ni). The reaction of $M(NCS)_2(OCMe_2)_2$ (M = Cr, Mn) in MeCN and $[Co(NCMe)_6](BF_4)_2$ and KSCN in acetone and after diffusion of diethyl ether form $M(NCS)_2(Sol)_2$ that structurally differ as they form one-dimensional (1-D) (M = Co; Sol = THF), two-dimensional (2-D) (M = Mn; Sol = MeCN), and three-dimensional (3-D) (M = Cr; Sol = MeCN) extended structures. 1-D $Co(NCS)_2(THF)_2$ has *trans*-THFs, while the acetonitriles have a *cis* geometry for 2- and 3-D $M(NCS)_2(NCMe)_2$ (M = Cr, Mn). 2-D $Mn(NCS)_2(NCMe)_2$ is best described as $Mn^{II}(\mu_{N,N}\text{-NCS})(\mu_{N,S}\text{-NCS})(NCMe)_2$ [= $Mn_2(\mu_{N,N}\text{-NCS})_2(\mu_{N,S}\text{-NCS})_2(NCMe)_4$] with the latter $\mu_{N,S}$-NCS providing the 2-D connectivity. In addition, the reaction of $Fe(NCS)_2(OCMe_2)_2$ and 7,7,8,8-tetracyanoquino-*p*-dimethane (TCNQ) forms 2-D structured $Fe^{II}(NCS)_2TCNQ$. The magnetic behavior of 1-D $Co(NCS)_2(THF)_2$ can be modeled by a 1-D Fisher expression ($H = -2JS_i \cdot S_j$) with g = 2.4 and J/k_B = 0.68 K (0.47 cm^{-1}) and exhibit weak ferromagnetic coupling. $Cr(NCS)_2(NCMe)_2$ and $Fe^{II}(NCS)_2TCNQ$ magnetically order as antiferromagnets with T_c's of 37 and 29 K, respectively, while $Mn(NCS)_2(NCMe)_2$ exhibits strong antiferromagnetic coupling. $M(NCS)_2(THF)_4$ and $K_4[M(NCS)_6]$ (M = V, Ni) are paramagnets with weak coupling between the octahedral metal centers.

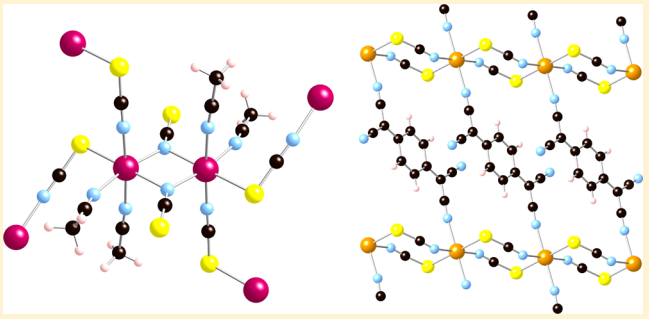

INTRODUCTION

Thiocyanate is a commonly used ligand because of its numerous bonding modes to one or more transition metal ions, and provides useful precursors for numerous coordination complexes.[1,2] Usually, thiocyanate terminally bonds through the nitrogen with first row transition metals. Additionally, bridging thiocyanates with the M-NCS-M motif form compounds of $M(NCS)_2Sol_2$ (Sol = solvent) composition with extended one-dimensional (1-D) and two-dimensional (2-D) structures.[3,4] Other bonding possibilities are known, such as three-way bridging (>SCN-) or (-SCN<),[5] but are uncommon. Free NCS^- exhibits a ν_{NCS} at 2054 cm^{-1}, and two δ_{NCS} bending modes at 486 and 471 cm^{-1}. Upon binding to a metal ion, the δ_{NCS} doublet typically becomes a singlet and shifts to lower frequency (~480 cm^{-1}) for an M-N bond, and lower for an M-S bond (~420 cm^{-1}).[1] When thiocyanate bridges two metal centers ($\mu_{N,S}$-NCS^-), two δ_{NCS} absorptions for both M-N and M-S are present. Fe^{III} seems to have a strong preference to form octahedral complexes with thiocyanate despite our efforts to control and form tetrahedral complexes.

Previously, we reported several acetone solvates and their reaction with $(NBu_4)(TCNE)$ (TCNE = tetracyanoethylene) that formed extended three-dimensional (3-D) network structures of $M(TCNE)[C_4(CN)_8]_{1/2}\cdot zCH_2Cl_2$ and $M[C_4(CN)_8]\text{-}(Sol)_2$ compositions.[4] Due to their utility to develop new inorganic compounds and materials, herein the reaction of several first row transition metal complexes with KSCN in acetone, as well as the reaction of $M^{II}(NCS)_2(acetone)_2$ (M = Cr, Mn) in acetonitrile is explored, and several bridging thiocyanate-based complexes of $M^{II}(NCS)_2(Sol)_x$ (x = 2; 4) (M = Fe, Mn, Cr, Co, V; Sol = MeCN, THF) composition have been prepared. In addition, $K_4[M^{II}(NCS)_6]\cdot 0.25(OCMe_2)$ (M = V, Ni) have been prepared, and we report their structures and magnetic properties. $Fe^{II}(NCS)_2TCNQ$ has also been prepared from the reaction of $Fe(NCS)_2(OCMe_2)_2$ and 7,7,8,8-tetracyanoquino-*p*-dimethane (TCNQ).

All of these materials have been structurally characterized and vary from homolytic tetrahedral and octahedral thiocyanate

Received: June 21, 2013
Published: August 27, 2013

   dx.doi.org/10.1021/ic401558f | *Inorg. Chem.* 2013, 52, 10583−10594

complexes to 2-D and 3-D network structures with bridging thiocyanates. These structures have magnetic properties that vary from paramagnetic to antiferromagnets and are discussed herein.

EXPERIMENTAL SECTION

Metal(II) chlorides (Strem Chemicals), $(NMe_4)Br$, $FeCl_2$, and KSCN (Sigma-Aldrich) were used as purchased without any further purification. $V^{II}SO_4$ was prepared as described in the literature.[6] $[M^{II}(NCMe)_6](BF_4)_2$ (M = V, Fe, Co) and $M(NCMe)_4(BF_4)_2$ (M = Cr, Mn) were prepared as described in the literature[7] from metal(II) chlorides and $AgBF_4$ using acetonitrile as solvent. $M(NCS)_2(OCMe_2)_2$ (M = Cr, Mn, Fe)[4] and $K_2[Co(SCN)_4]$[8] were prepared as described previously. 7,7,8,8-Tetracyano-*p*-quinodimethane was a gift from the Du Pont Co. The preparation of $(NMe_4)NCS$ was carried under ambient conditions, while all other syntheses were performed under dry N_2 atmosphere in a Vacuum Atmospheres DriLab (<1 ppm O_2). Acetonitrile was purified through an activated alumina dual-column purification system under a positive pressure of dry N_2. Diethyl ether (Et_2O) and acetone (Me_2CO) were distilled from appropriate drying agents under dry N_2.

$(NMe_4)SCN$. $(NMe_4)Br$ (6.40 g, 41.1 mmol) and KSCN (4.00 g, 41.1 mmol) were each dissolved in 50 mL of absolute ethanol. The KSCN solution was rapidly added into the $(NMe_4)Br$ solution while stirring, and a white precipitate immediately formed. After stirring for 30 min, the mixture was filtered, and the clear solution was evaporated using rotary evaporation. A white solid was obtained (Yield: 4.64 g, 85%). IR (KBr): ν_{CH} 3026 (m), ν_{CN} 2058 (s), ν_{SC} 741 (s) cm^{-1}. The standard one-electron reduction potential is 533 mV vs SCE in acetonitrile.

$(NMe_4)_2[Fe^{II}(NCS)_4]\cdot MeCN$, 1. $FeCl_2$ (500 mg, 3.94 mmol) was dissolved in ~15 mL of acetonitrile. KSCN (767 mg, 7.88 mmol) dissolved in 5-mL acetonitrile was quickly added to the $FeCl_2$ solution, an immediate white precipitate formed, and the solution turned brown. After stirring for 30 min, it was filtered through Celite to remove the precipitate. $(NMe_4)SCN$ (1.05 g, 7.96 mmol) dissolved in 10-mL of acetonitrile was quickly added to the $FeCl_2$ solution. The dark orange mixture was stirred overnight. The mixture was taken to dryness. (Yield 1.34 g, 71%). Complex **1** was dissolved in a small amount of acetonitrile, and upon diffusion with Et_2O led to the formation of light purple crystals. Some crystals were collected and stored in the presence of mother liquor for characterization with a single crystal X-ray diffraction. IR (KBr): ν_{CH} 3028 (m), ν_{CN} 2308 (w), 2252 (w), ν_{SCN} 2066 (s), δ_{NCS} 479 (m) cm^{-1}. The diamagnetic correction is -272×10^{-6} emu/mol.

$(NMe_4)_2[Co^{II}(NCS)_4]$, 2. $(NMe_4)SCN$ (0.5 g; 0.375 mmol) was dissolved in 15 mL of warm EtOH. A solution of 0.70 g of $K_2[Co(SCN)_4]$ in 15 mL of EtOH was slowly added to the $[NMe_4][SCN]$ solution, and a light blue precipitate formed. The reaction was filtered leaving bright blue solids and a blue filtrate; 0.87 g collected, 91% yield. IR (KBr): ν_{SCN} 2105 (sh), 2076 (s), δ_{NCS} 478 (w) cm^{-1}. The diamagnetic correction is -243×10^{-6} emu/mol.

$Fe^{II}(NCS)_2(NCMe)_4$, 3. $FeCl_2$ (300 mg, 2.34 mmol) was dissolved in a small amount of acetonitrile (5 mL). KSCN (460 mg, 4.68 mmol) was also dissolved in 5 mL of acetonitrile and added quickly to the $FeCl_2$ solution. An immediate white precipitate formed (KCl). The solution was stirred for 30 min and filtered through Celite to remove the precipitate. The clear solution was taken to dryness (Yield 531 mg, 66%). Compound **3** was redissolved in a small amount of acetonitrile, and diffusion with Et_2O led to the formation of colorless crystals. Some crystals were collected and stored in the presence of mother liquor for characterization with a single crystal X-ray diffraction. IR (KBr): ν_{CH} 2987 (m), 2927 (m), ν_{CN} 2311 (s), 2289 (s), 2099 (s), ν_{Me} 1366 (m), 1028 (m), 938 (m), δ_{NCS} 477 (m), 467 (m) cm^{-1}. The diamagnetic correction is -186×10^{-6} emu/mol.

$Cr^{II}(NCS)_2(NCMe)_2$, 4. $Cr(NCS)_2(OCMe_2)_2$ (500 mg; 1.76 mmol) was dissolved in acetonitrile. The Et_2O diffusion technique was used to obtain a purple powder of **4** (387 mg, 66%). IR (KBr): ν_{CH} 2990 (m), 2922 (m), ν_{CN} 2316 (m), 2293 (m), 2105 (sh), 2096 (s), δ_{NCS} 478 (w), 468 (w), cm^{-1}. The diamagnetic correction is -183×10^{-6} emu/mol.

$Mn^{II}(NCS)_2(NCMe)_2$, 5. $Mn(NCS)_2(OCMe_2)_2$ (200 mg; 0.70 mmol) was dissolved in acetonitrile. The Et_2O diffusion technique was used to obtain transparent crystals of **5** (135 mg, 77%). IR (KBr): ν_{CH} 2988 (m), 2924 (m), 2834 (m), ν_{CN} 2300 (s), 2273 (s), 2109 (s), 1998 (s), δ_{NCS} 490 (m), 476 (m), 461 (m) cm^{-1}. The diamagnetic correction is -132×10^{-6} emu/mol.

$Co^{II}(NCS)_2(THF)_2$, 6. $[Co(NCMe)_6](BF_4)_2$ (600 mg, 1.25 mmol) was dissolved in 10 mL of acetone. KSCN (244 mg, 2.50 mmol), dissolved in 10 mL of acetone, was quickly added to the above solution, and an immediate white precipitate formed (KBF_4) and the solution turned blue. After stirring overnight, the mixture was filtered through Celite to remove the precipitate, and the filtrate was taken to dryness (Yield 253.6 mg, 87%). Diffusion of tetrahydrofuran (THF) in acetone solution led to formation of purple crystals. IR (KBr): ν_{CH} 2981 (m), 2887 (m), ν_{CN} 2113 (s), ν_{THF} 1457 (m), 1362 (m) 1339 (m), 1296 (m), 1238 (m), 1176 (m), 1036 (s), 922 (s), 878 (s,b), 677 (m), δ_{NCS} 477 (w) cm^{-1}. The diamagnetic correction is -294×10^{-6} emu/mol.

$V^{II}(NCS)_2(THF)_4$, 7. $[V(NCMe)_6](BF_4)_2$ (300 mg, 0.637 mmol) was dissolved in 5 mL of acetone. KSCN (124 mg, 1.27 mmol) was also dissolved in 5 mL of acetone and added quickly to the dark orange $[V(NCMe)_6](BF_4)_2$ solution. An immediate white precipitate formed (KBF_4), and the solution turned dark brown. After stirring overnight, the brown mixture was filtered through Celite to remove the precipitate. The solution was taken to dryness and redissolved in acetone (Yield 124.8 mg, 87%). **7** was redissolved in a small amount of acetone, and THF diffusion was used to obtain brown crystals. IR (KBr): ν_{CH} 2979 (m), 2893 (m). ν_{CN} 2072 (s), ν_{THF} 1459 (m), 1368 (w), 1300 (w), 1242 (m), 1180 (w), 1036 (s), 922 (s), 882 (s,b), 677 (m), δ_{NCS} 483 (w) cm^{-1}. The diamagnetic correction is -285×10^{-6} emu/mol.

$Ni^{II}(NCS)_2(THF)_4$, 8. $NiCl_2$ (200 mg, 1.54 mmol) was suspended in 10 mL of acetone, and KSCN (300 mg, 3.08 mmol) also dissolved in 5 mL of acetone was quickly added. After stirring overnight, the green mixture was filtered through Celite to remove the precipitate (KBF_4). THF/Et_2O diffusion yielded green single crystals (Yield 460 mg, 65%). IR (KBr): ν_{CH} 2978 (m), 2884 (m), ν_{CN} 2127 (s), 2083 (sh), ν_{THF} 1459(m), 1039 (m), 922 (m), 881 (m), δ_{NCS} 471 (m) cm^{-1}. The diamagnetic correction is -281×10^{-6} emu/mol.

$K_4[V^{II}(NCS)_6]\cdot 0.25(Me_2CO)$, 9. $V^{II}SO_4$ (300 mg, 2.04 mmol) was suspended in 20 mL of acetone. KSCN (397 mg, 4.08 mmol) was also dissolved in 5 mL of acetone and added quickly to the yellow vanadium sulfate mixture. An immediate tan precipitate formed, and the solution turned dark orange. The solution was stirred overnight. The brown mixture was filtered through Celite to remove the precipitate. The solution was taken to dryness and redissolved in acetone (Yield 200 mg, 53%). **9** was redissolved in a small amount of acetone, and Et_2O diffusion was used to obtain dark green crystals. IR (KBr): ν_{CN} 2115 (s), δ_{NCS} 479 (m) cm^{-1}. Anal. Calcd. for $C_6K_4N_6S_6V$: C, 12.97; N, 15.12; S, 34.61. Found: C, 13.17; N, 15.25; S, 33.88%. The diamagnetic correction is -259×10^{-6} emu/mol. The density was determined to be 1.658 g/cm^3.

$K_4[Ni^{II}(NCS)_6]\cdot 0.25(Me_2CO)$, 10. $NiCl_2$ (580 mg, 4.48 mmol) was suspended in 10 mL of acetone. KSCN (870 mg, 8.95 mmol) was dissolved in 5 mL of acetone and added to the $NiCl_2$ slurry solution, and the mixture turned immediately blue, and was stirred overnight. The mixture was filtered through Celite to remove the precipitate. The solution was taken to dryness, and a green solid was obtained (yield 650 mg, 25%). IR (KBr):ν_{CN} 2129 (s), 2093 (sh), δ_{NCS} 471 (m) cm^{-1}. The diamagnetic correction is -256×10^{-6} emu/mol.

$Fe^{II}(NCS)_2TCNQ$, 11. $Fe(NCS)_2(OCMe_2)_2$ (41 mg, 0.142 mmol) was suspended in 5 mL of CH_2Cl_2. 7,7,8,8-Tetracyanoquino-*p*-dimethane (TCNQ) (59 mg, 0.284 mmol) was dissolved in 10 mL of CH_2Cl_2 forming a yellow solution and was added to the compound $Fe(NCS)_2(OCMe_2)_2$ suspension quickly. The reaction was allowed to stir overnight. The black mixture was filtered, and the black precipitate washed with a small amount of CH_2Cl_2 (Yield 50.3 mg, 94%). A small sample was packed in quartz capillary for powder X-ray diffraction (XRD). IR (KBr): ν_{CH} 3041 (m), ν_{CN} 2241 (m), 2223 (m), 2142 (m), 2095 (s), δ_{NCS} 476 (m), 466 (m) cm^{-1}. The diamagnetic correction is -173×10^{-6} emu/mol.

Physical Measurements. Infrared spectra were recorded from 400 to 4000 cm^{-1} on a Bruker Tensor 37 infrared spectrophotometer (± 1 cm^{-1}) with a KBr pellet. Electrochemical experiments were performed under inert atmosphere with a Bioanalytics eEpsilon

dx.doi.org/10.1021/ic401558f | Inorg. Chem. 2013, 52, 10583−10594

Table 1. Diagnostic IR Peaks and Crystal Color for Compounds 1−11

compound	M^{II}	ν_{CN} (cm^{-1})	ν_{CO} (cm^{-1})	δ_{NCS} (cm^{-1}) M-N	color
1	Fe	2308 (w), 2252 (w), 2066(s)		479 (m)	purple
2	Co	2105 (sh), 2076 (s)		478 (w) 468 (w)	light blue
3	Fe	2311 (s), 2289 (w), 2099 (s)		477 (m) 467 (m)	colorless
4	Cr	2316 (m), 2293 (m), 2105 (sh), 2096 (s)		478 (w) 468 (w)	purple
5	Mn	2300 (s), 2273 (s), 2109 (s), 1998 (s)		490 (w) 476 (w) 461 (w)	colorless
6	Co	2113 (s)	1036 (s), 922 (s), 878 (s)[a]	477 (w)	purple
7	V	2072 (s)	1036 (s), 922 (s), 882 (s)[a]	483 (w)	brown
8	Ni	2127 (s), 2083 (sh)	1039 (m), 922 (m), 881 (m)[a]	471 (w)	green
9	V	2115 (s)	1705 (m)[b]	479 (w)	dark green
10	Ni	2129 (s), 2093 (sh)	1705 (m)[b]	471 (m)	green
11	Fe	2241(s), 2142(s), 2095(s)		471 (m)	black

[a]From THF. [b]From Me_2CO.

instrument. The reference electrode was $Ag/AgNO_3$ with a 0.01 M $(NBu_4)(PF_6)$ supporting electrolyte in acetonitrile. All the samples were diluted to 5 mM, and ferrocene was used as a standard. The working electrode was Pt.

Magnetic susceptibility measurements were made between 2 to 300 K using a Quantum Design MPMS-5 5T SQUID magnetometer with a sensitivity of 10^{-8} emu or 10^{-12} emu/Oe at 1 T and equipped with the ultralow field (~0.005 Oe), reciprocating sample measurement system, and continuous low temperature control with enhanced thermometry features, as previously reported.[9] Diamagnetic corrections were determined from Pascal's constants.[10] X-Band EPR spectra were recorded on a Bruker EMX-EPR spectrometer. Density measurements were performed under inert atmosphere by utilizing mixture of dichloromethane and dibromomethane.

The crystal structures of **1**, **3**, **5**, **6**, **7**, and **8** were determined from single crystals on a Bruker APEX CCD diffractometer. All the reflections were merged, and only those for which $I_o > 2\sigma(I)$ were included in the refinement, were $\sigma(F_o)^2$ is the standard deviation based on counting statistics. The data were integrated using the Bruker SAINT software program.[11] The structures were solved by Patterson methods and refined by full-matrix least-squares methods using SHELXL-97. All the non-hydrogen atoms were refined with anisotropic displacement coefficients. Hydrogen atoms were assigned isotropic displacements $U(H) = 1.2U(C)$, and their coordinates were allowed to ride on their respective carbons using SHELXL97.[12]

High-resolution powder diffraction measurements for structural analysis of compounds **2**, **4**, **9**, **10**, and **11** were performed at beamline X16C of the National Synchrotron Light Source at Brookhaven National Laboratory. The powdered samples were sealed in nominal 1.0 mm diameter thin-wall quartz capillaries. X-rays were selected by a channel-cut Si(111) monochromator. Diffracted X-rays were selected by a Ge(111) analyzer and detected by a NaI scintillation counter. The capillary was spun at several Hz during data collection to improve particle statistics. The incident intensity was monitored by an ion chamber and used to normalize the measured signal. TOPAS-Academic was used to index, solve, and refine the crystal structures.[13−15] Rietveld plots are given in the Supporting Information.

RESULTS AND DISCUSSION

The reaction of $FeCl_2$ with 2 equiv each of KSCN and $(NMe_4)SCN$ formed purple $(NMe_4)_2[Fe^{II}(NCS)_4]\cdot MeCN$ (**1**). Goodgame et al. proposed a tetrahedral iron(II) complex, but did not report a crystal structure.[16] The ν_{CN} absorptions at 2308 and 2252 cm^{-1} are characteristic of uncoordinated acetonitrile solvent, while the 2066 cm^{-1} peak is characteristic for terminally bound thiocyanate, and the 479-cm^{-1} absorption is assigned to the M-N bond from the bending mode of NCS ligand.[17] The Co^{II} analogue $(NMe_4)_2[Co^{II}(NCS)_4]$ was prepared from the reaction of $(NMe_4)_2[Co^{II}(NCS)_4]$ and (NMe4)NCS in EtOH. In contrast, the reaction of $FeCl_2$ and 2 equiv of KSCN in acetonitrile formed $Fe(NCS)_2(NCMe)_4$ (**3**) with ν_{SCN} absorption at 2276 cm^{-1} corresponding to the terminal N-bonded thiocyanate ligand in accord with that observed for **1**.

To determine if $[Fe^{II}(NCS)_4]^{2-}$ could be reversibly oxidized to $[Fe^{III}(NCS)_4]^{-}$, cyclic voltammetry measurements were performed, but no reversible oxidation was observed. Furthermore, $[Fe^{II}(NCS)_4]^{2-}$ does not react with either TCNE or $[TCNE]^{\bullet-}$.

$M(NCS)_2(OCMe_2)_2$ (Mn = Cr, Mn) was dissolved in acetonitrile to form $M(NCS)_2(NCMe)_2$ [M = Cr (**4**), Mn (**5**)]. The ν_{CN} absorptions at 2316 and 2293 cm^{-1} of **4** are characteristic of coordinated acetonitrile. The other two ν_{CN} absorptions at 2105 and 2096 cm^{-1} suggest coordinated thiocyanate ligands. Two δ_{NCS} and δ_{NCC} absorptions at 478 and 468 cm^{-1} suggest M-N(CS) and M-N(CMe) bonding.

Similarly, compound **5** has ν_{CN} absorptions at 2300 and 2273 cm^{-1} suggesting coordinated acetonitrile. Only one ν_{CN} absorption is observed at 2109 cm^{-1} suggesting bridging thiocyanate (-NCS-). The ν_{CN} absorption at 1998 cm^{-1} suggests a μ_3-NCS (>NCS-). Three bending modes are observed at 490, 476, and 461 cm^{-1} suggesting three types of M-N bonds.

$Co(NCS)_2(THF)_2$ (**6**), $V(NCS)_2(THF)_4$ (**7**), and $Ni(NCS)_2(THF)_4$ (**8**) were prepared in attempts to grow single crystals of $M(NCS)_2(OCMe_2)_2$ (M = Co, V, Ni, respectively) using THF/acetone diffusion. The ν_{CN} absorption for **6** occurred at 2113 cm^{-1} suggesting a bridged thiocyanate, while it occurs at 2072 cm^{-1} for **7** suggesting only an *N*-bound thiocyanate. The ν_{CN} absorption for **8** occurred at 2127 cm^{-1} suggesting a bridged thiocyanate. All three compounds have δ_{NCS} at 477, 483, and 471 cm^{-1}, respectively, in accord with an M-N bond. Absorption frequencies for THF have been observed for all three compounds and a few of them are reported in Table 1.

The reaction of VSO_4 and KSCN in acetone forms $K_4[V(NCS)_6]\cdot 0.25(OCMe_2)$ (**9**) that was crystallographically characterized. The ν_{CN} 2115 cm^{-1} and δ_{NCS} for M-N at 479 cm^{-1} absorptions suggest *N*-bound thiocyanates, even though the ν_{CN} is above 2100 cm^{-1}. These values are in accord with 2107 and 475 cm^{-1} reported for $K_4[V(NCS)_6]\cdot EtOH$.[18] The ν_{CN} is significantly blue-shifted from 2078 ± 13 cm^{-1}, and slightly blue-shifted from 484 ± 4 cm^{-1} that is observed for $A_4[V(NCS)_6]$ (A = NMe_4^+, NEt_4^+, $NHex_4^+$, Hpy^+; py = pyridine).[19] The blue shift is due to the cation···S interactions, and is consistent with that observed for hexacyanometallates.[20] The 1705-cm^{-1} ν_{CO} peak indicates lattice-trapped acetone, as it lies between that of free (1720 cm^{-1}) and coordinated acetone at (~1680 cm^{-1}).

The slurry reaction of $NiCl_2$ and KSCN forms $K_4[Ni(NCS)_6]\cdot 0.25(OCMe_2)$ (**10**) with absorptions at 2129, 2093, and 471 cm^{-1}.

dx.doi.org/10.1021/ic401558f | Inorg. Chem. 2013, 52, 10583−10594

Table 2. Summary of the Crystallographic Parameters of Compounds 1 to 11

compound	$(NMe_4)_2[Fe(NCS)_4]\cdot MeCN$	$(NMe_4)_2[Co(NCS)_4]$	$Fe^{II}(NCS)_2(NCMe)_4$	$Cr^{II}(NCS)_2(NCMe)_2$	$Mn^{II}(NCS)_2(NCMe)_2$	$Co^{II}(NCS)_2(THF)_2$	$V^{II}(NCS)_2(THF)_4$	$Ni^{II}(NCS)_2(THF)_4$	$K_4V^{II}(NCS)_6\cdot 0.25(OCMe_2)$	$K_4Ni^{II}(NCS)_6\cdot 0.25(OCMe_2)$	$Fe^{II}(NCS)_2$-TCNQ
designation	**1**	**2**	**3**	**4**	**5**	**6**	**7**	**8**	**9**	**10**	**11**
empirical formula	$C_{14}H_{27}FeN_7S_4$	$C_{12}H_{24}CoN_6S_4$	$C_{10}H_{12}FeN_6S_2$	$C_6H_6CrN_4S_2$	$C_6H_6MnN_4S_4$	$C_{30}H_{48}Co_3N_6O_6S_6$	$C_{18}H_{32}N_2O_4S_2V$	$C_{18}H_{32}N_2NiO_4S_2$	$C_{6.75}H_{1.5}K_4N_6O_{0.25}S_6V$	$C_6K_4N_6NiS_6$	$C_{14}H_4FeN_6S_2$
MW, g/mol	477.52	439.58	336.23	250.26	253.21	957.89	455.52	463.29	570.35	563.58	370.20
T (K)	150(1)	298(1)	100(2)	298(1)	113(2)	150(1)	150(1)	120(2)	298(2)	298(2)	298(1)
a (Å)	10.8727(2)	24.6433(2)	10.7457(7)	9.08966(13)	9.0889(13)	10.0641(10)	15.2033(3)	14.9647(8)	8.45880(2)	8.15111(2)	5.5742(1)
b (Å)	10.96200(10)	11.30658(11)	10.7457(7)	9.16685(11)	9.0476(13)	10.2026(9)	10.0157(2)	9.9927(5)	8.45880(2)	8.15111(2)	6.13885(12)
c (Å)	12.5335(2)	24.9333(3)	14.4185(13)	12.6894(2)	13.1775(18)	11.1551(11)	16.1131(3)	15.9621(8)	9.19365(4)	9.16677(2)	11.4552(3)
α (deg)	111.0992(9)	90	90	90	90	70.675(7)	90	90	90	90	78.4226(8)
β (deg)	112.9976(8)	94.7301(9)	90	90	104.994(2)	71.120(5)	111.6140(13)	112.0140(10)	90	90	80.0358(8)
γ (deg)	97.0445(10)	90	90	90	90	77.773(6)	90	90	120.00	120	78.2382(15)
V (Å^3)	1221.13(3)	6923.52(12)	1664.9(2)	1057.32(3)	1046.7(3)	1015.67(17)	2281.05(8)	2212.9(2)	569.687(3)	566.989(18)	372.365(14)
Z	2	12	4	4	4	1	4	4	1	1	1
space group	$P\bar{1}$	$C2/c$	$P4_32_12$	$P2_12_12_1$	$P2_1/n$	$P\bar{1}$	$P2_1/c$	$P2_1/c$	$P6_3/mcm$	$P6_3/mcm$	$P\bar{1}$
ρ, calc (g cm^{-3})	1.2987	1.265	1.341	1.572	1.607	1.566	1.326	1.391	1.67[c]	1.65	1.678
wavelength, λ, Å	0.71073	0.700154	0.71073	0.69977	0.71073	0.71073	0.71073	0.71073	0.69730	0.99974	0.700154
R1 $[I>2\sigma(I)]$[a]	0.0302		0.0437		0.0242	0.0606	0.0570	0.0308			
wR2 $[I>2\sigma(I)]$[b]	0.0698		0.1073		0.0783	0.1674	0.1493	0.0712			
goodness of fit (F^2)	1.044	2.031	1.073	1.301	1.073	1.106	1.044	1.060	2.324	3.55	1.346
largest diff. peak/hole, e$^-$ Å^{-3}	0.383		0.597			1.715	0.710	0.518			
R_{wp}[d,e]		0.0657		0.0664					0.0606	0.0586	0.0831
R_{exp}[e,f]		0.0323		0.0510					0.0261	0.0165	0.0617
CCDC#	806643	945401	806646	945402	945403	806644	806642	806648	945404	945405	945406

[a] $R_1 = \sum||F_o| - |F_c||/\sum|F_o|$. [b] $wR_2 = [\sum w(F_o^2 - F_c^2)^2/\sum w(F_o^2)^2]^{1/2}$. [c] Observed density is 1.658 g/cm^3. [d] $R_{wp} = ((\sum_i w_i(y_i^{calc} - y_i^{obs})^2)/((\sum_i w_i(y_i^{obs})^2))^{1/2}$. [e] y_i^{calc} and y_i^{obs} are the calculated and observed intensities at the ith point in the profile, normalized to monitor intensity. The weight w_i is $1/\sigma^2$ from the counting statistics, with the same normalization factor. N is the number of points in the measured profile minus number of parameters. [f] $R_{exp}((N)/((\sum_i w_i(y_i^{obs})^2))$.

dx.doi.org/10.1021/ic401558f | Inorg. Chem. 2013, 52, 10583−10594

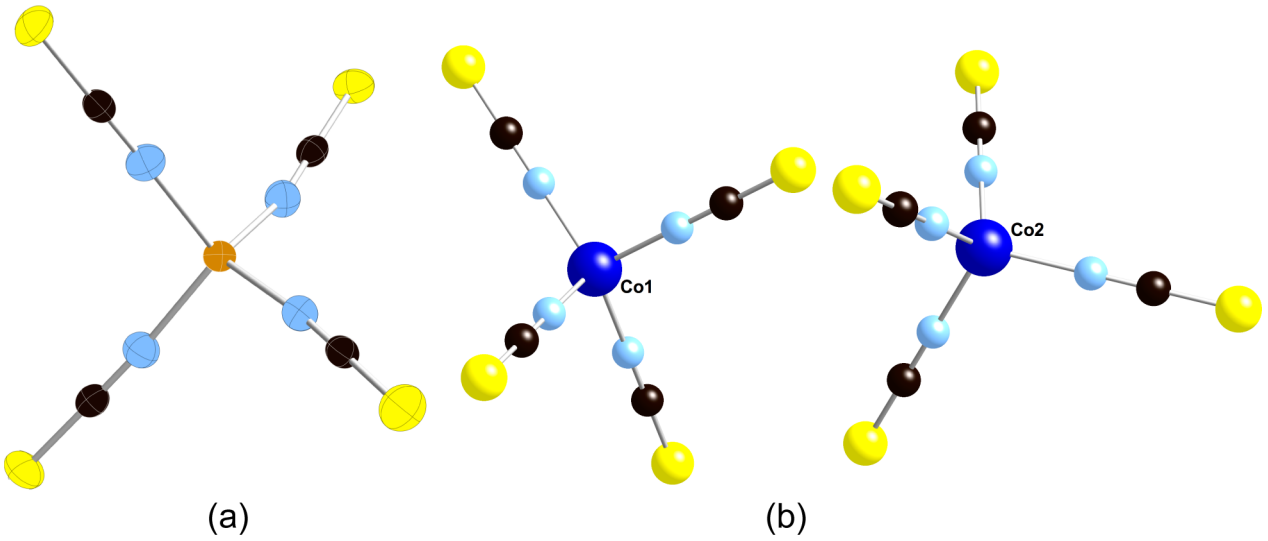

Figure 1. Atom labeling ORTEP drawing (50% probability thermal ellipsoids) of $[Fe(NCS)_4]^{2-}$ present in $(NMe_4)_2[Fe(NCS)_4]$·MeCN (**1**) (a). The two crystallography different $[Co(NCS)_4]^{2-}$ ions present in $(NMe_4)_2[Co(NCS)_4]$ (**2**) (b). Isotropic thermal parameters were used for **2**, as thermal ellipsoids could not be reliably determined from the available PXRD data.[25]

These frequencies are blue-shifted from 2109, 2102, and 460 cm^{-1} for the previously reported $(NEt_4)_4[Ni(NCS)_6]$[1] again because of the $K^+\cdots S$ interactions.[20] (A ν_{CN} of 2098 cm^{-1} was also reported for $(NEt_4)_4[Ni(NCS)_6]$.[21]) The ν_{CN} 2129 cm^{-1} and δ_{NCS} for M-N at 471 cm^{-1} absorptions suggest *N*-bound thiocyanates, even though the ν_{CN} is above 2100 cm^{-1}. There is also lattice-trapped acetone indicated from the ν_{CO} peak at 1704 cm^{-1}.

The slurry reaction of $Fe(NCS)_2(OCMe_2)_2$ and TCNQ forms $Fe(NCS)_2TCNQ$ (**11**) with ν_{CN} absorptions at 2241, 2142, and 2095 cm^{-1}. The first two absorptions suggest coordinated neutral TCNQ°, as occurs for $[Ru_2Piv_4(H_2O)_2TCNQ](BF_4)_2$ (Piv = pivalate; *t*-$BuCO_2^-$),[22] while the third absorption suggests coordinated thiocyanate.

Structures. The structures of **1**, **3**, **5**, **6**, **7**, and **8** were determined by single crystal X-ray analyses, while **2**, **4**, **9**, **10**, and **11** were determined by powder X-ray analysis. A summary of all crystallographic parameters is provided in Table 2.

The structure of **1** was determined to be $(NMe_4)_2[Fe^{II}(NCS)_4]$·MeCN. The Fe^{II} is tetrahedral with Fe−N bond lengths ranging from 1.997(2) to 2.002(2) Å, and averaging 1.999 Å. This average Fe−N bond length is very similar to the 2.032 Å Fe^{II}−N bond length in $[Ru^{II}(phen)_3]_2[Fe^{II}(NCS)_4]$·2NCS·4$H_2O$ (phen = *o*-phenanthroline), which is also in a tetrahedral environment.[23] The C−S and C≡N bond lengths average 1.620 and 1.163 Å, respectively. The C≡N distance is in accord with that observed for KSCN; however, the C−S distance is 0.06 Å shorter than observed for KSCN.[24] The tetrahedral iron centers are grouped in pairs, with the next nearest neighbor Fe···Fe being 7.529 Å. The shortest distance between iron centers is 7.267 Å. The ν_{CN} for **1** occurs at 2066 cm^{-1} in accord with terminal thiocyanates. The absence of δ_{NCS} for M-S and the presence of only δ_{NCS} for M-N at 479 cm^{-1} agree with the thiocyanate being *N*-bound.

The structure of **2** was determined to be $(NMe_4)_2[Co^{II}(NCS)_4]$. It has a large unit cell with 12 molecules per the unit cell, 2 being unique. The Co^{II} has a tetrahedral geometry with an average Co−N bond length of 1.942 Å. The C−S and C≡N bond lengths average 1.539 and 1.150 Å, respectively. The shortest Co···Co distance is 7.785 Å. The structures of each of the two independent tetrahedral $[Co^{II}(NCS)_4]^{2-}$ ions are similar to that of $[Fe^{II}(NCS)_4]^{2-}$, Figure 1.

Compound **3** was determined to be *trans*-$Fe(NCS)_2(NCMe)_4$ (Figure 2). The octahedral Fe^{II} has Fe−N bond distances of

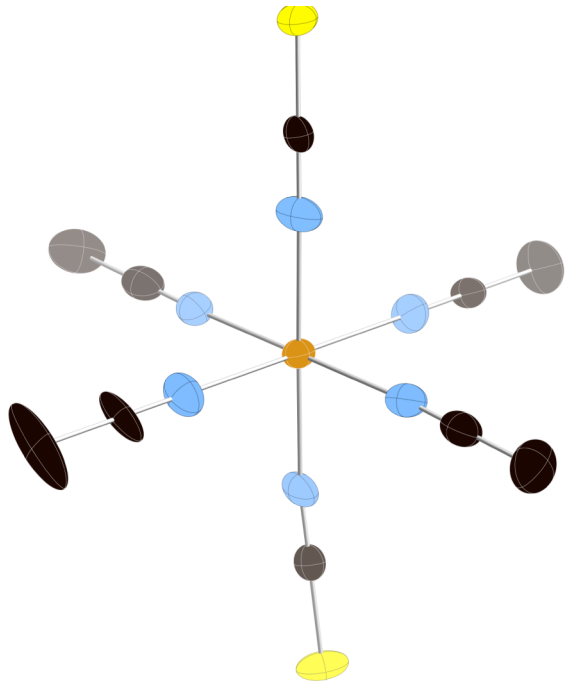

Figure 2. Atom labeling ORTEP drawing (50% probability thermal ellipsoids) of $Fe(NCS)_2(NCMe)_4$ (**3**); hydrogen atoms are omitted for clarity.

2.097(3) for Fe-NCS, and 2.154(5), 2.164(5), and 2.196(4) Å for Fe-NCMe suggesting a Jahn−Teller tetragonal elongation along the *trans*−Fe-N(CS) axis. This structure is in agreement with the 2311 and 2289 cm^{-1} ν_{CN} absorptions observed for the coordinated MeCN. These absorptions are shifted to higher energy, as expected when acetonitrile coordinates to metal centers.[26] The 2099 cm^{-1} ν_{CN} corresponds to terminal *N*-bonded thiocyanates. The 477 and 467 cm^{-1} absorptions are assigned to δ_{NCS} and δ_{NCMe}.

dx.doi.org/10.1021/ic401558f | *Inorg. Chem.* 2013, 52, 10583−10594

Compound **4** was determined to be *cis*-$Cr(NCS)_2(NCMe)_2$ (Figure 3). The Cr^{II} centers are coordinated to four Cr−N bonds and two Cr−S bonds. Two Cr−N bonds are due to coordinated acetonitrile, and have bond distances of 2.082(6) and 2.143(8) Å. The other two Cr−N bonds come from two bridging $\mu_{N,S}$-NCS with bond distances of 2.005(7) and 2.050(14) Å. The Cr−S bond distances are 2.892(6) and 3.050(14) Å. These bond lengths are comparable with the Cr−S bond length of 2.99 Å that is present in CrS.[27] Compound **4** exhibits a Jahn−Teller elongation along the Cr−S bonds. The *cis*-arrangement forms a 3-D extended lattice (Figure 3) with Cr···Cr distances of 5.796 and 5.825 Å.

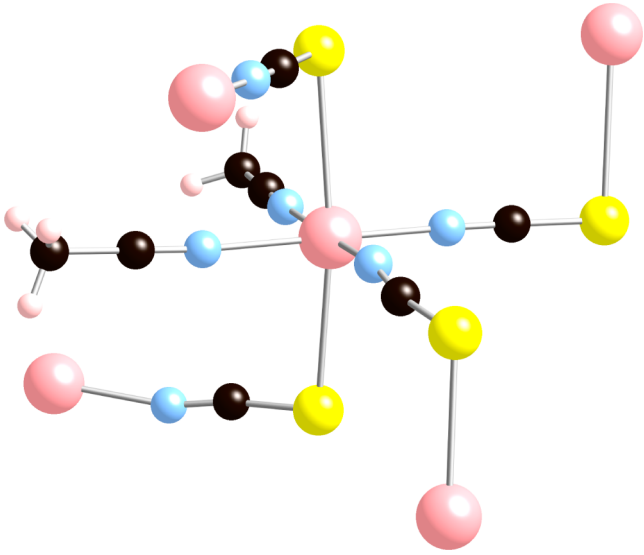

Figure 3. Extended 3-D network structure of $Cr(NCS)_2(NCMe)_2$, **4**; pink (Cr), blue (N), black (C), yellow (S). Isotropic thermal parameters were used, as thermal ellipsoids could not be reliably determined from the available PXRD data.

Compound **5** consists of $Mn(NCS)_2(NCMe)_2$. The Mn^{II} centers are coordinated with five Mn−N bonds and one Mn−S bond. The Mn^{II} center is bonded to two acetonitriles that are in a *cis*-orientation, two bridging $\mu_{N,N}$-thiocyanates, and two bridging $\mu_{N,S}$-thiocyanates (Figure 4). The two acetonitrile Mn−N bonds are 2.2340(17) and 2.2440(18) Å, while the two $\mu_{N,N}$-NCS Mn−N bonds are 2.2188(21) and 2.3189(17) Å, and the $\mu_{N,S}$-NCS Mn−N and Mn−S bonds are respectively 2.1449 (16) and 2.6716(8) Å. These two different bonding $\mu_{N,N}$- and $\mu_{N,S}$-thiocyanate motifs are in agreement with the ν_{CN} at 1998 and 2109 cm^{-1}, respectively. The overall structure consists of 2-D layers with $Mn^{II}(\mu_{N,N}\text{-NCS})(\mu_{N,S}\text{-NCS})(NCMe)_2$ [= $Mn_2(\mu_{N,N}\text{-NCS})_2(\mu_{N,S}\text{-NCS})_2(NCMe)_4$] repeat units, with the dimers connected via $\mu_{N,S}$-NCS. The intradimer Mn···Mn distance of 3.420(4) Å, and the shortest interlayer Mn···Mn distance is 8.172(5) Å. This structural motif differs from layered *trans*-$Mn(NCS)_2(HOEt)_2$ that only possesses $\mu_{N,S}$-NCS linkages.[28]

Compound **6** consists of a $Co(NCS)_2(THF)_2$ 1-D chain. The octahedral Co^{II} center is coordinated to two $\mu_{N,S}$-NCS forming a chain with two *trans*-THF molecules above and below the plane (Figure 5). The THF molecules have an AAB pattern along the

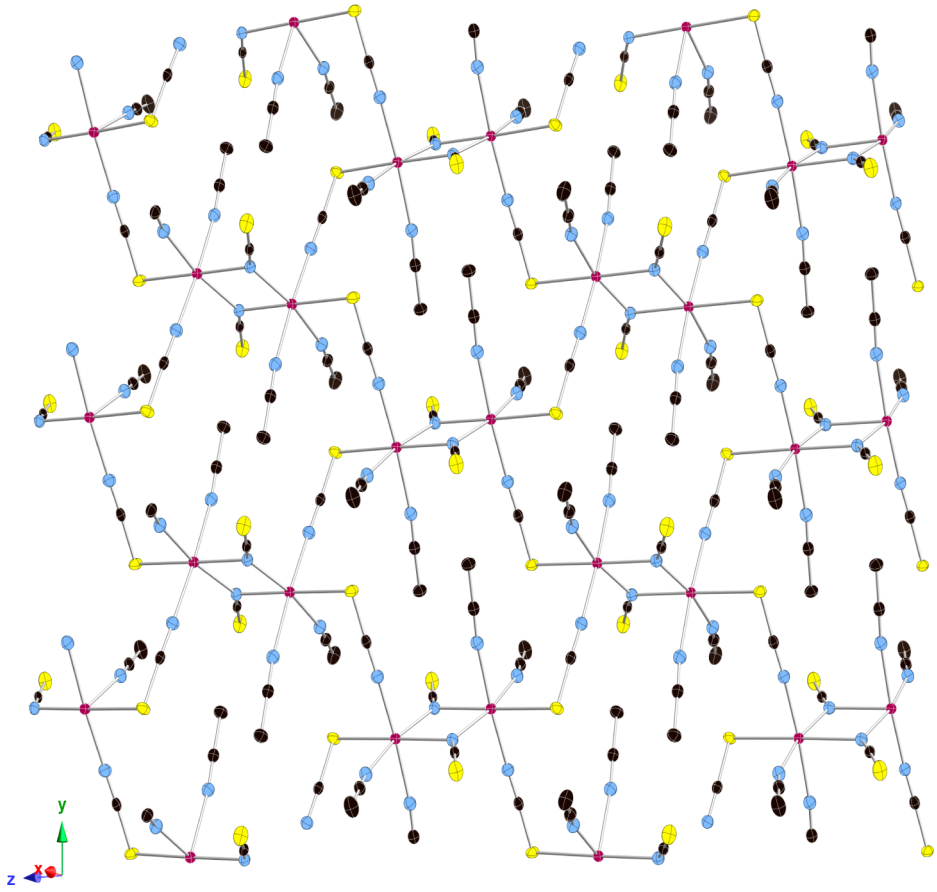

Figure 4. Atom labeling ORTEP drawing (50% probability thermal ellipsoids) of $Mn(NCS)_2(NCMe)_2$ (**5**); hydrogen atoms and labels are omitted for clarity. Each atom is depicted as purple (Mn), blue (N), black (C), and yellow (S); hydrogen atoms are omitted for clarity.

dx.doi.org/10.1021/ic401558f | *Inorg. Chem.* 2013, 52, 10583−10594

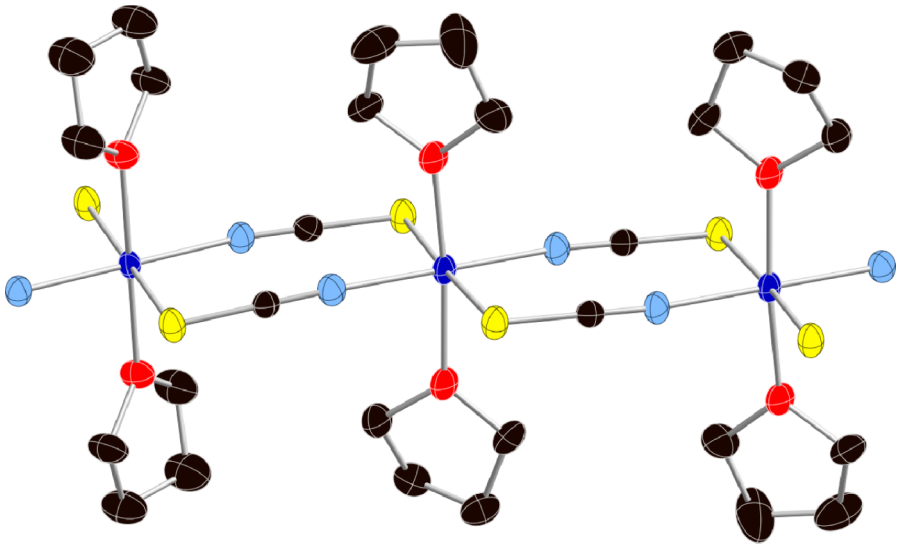

Figure 5. ORTEP drawing (50% probability thermal ellipsoids) structure of $Co(NCS)_2(THF)_2$ (**6**); dark blue (Co), blue (N), black (C), and yellow (S); hydrogen atoms are omitted for clarity.

1-D chain. The first two THFs are in the same plane as the direction of the 1-D chain, while the third THF is twisted 90° relative to the first two THFs, hence the AAB pattern. The bond distances are Co−N 2.049(7) Å, Co−S 2.563(5) Å, and Co−O 2.103(10) Å. The intrachain Co···Co distance is 5.634(21) Å, while the interchain distance is 7.554(30) Å.

Unlike for 2-D $Mn(NCS)_2(NCMe)_2$ (**5**) and 3-D $Cr(NCS)_2(NCMe)_2$ (**3**) whose extended structural motif have yet to be reported, the 1-D chain motif observed for $Co(NCS)_2(THF)_2$ (**6**) has been observed on numerous occasions, for example, $M(NCS)_2(OCMe_2)_2$,[4] $M(NCS)_2(py)_2$,[29] $MCl_2(py)_2$,[30] and $FeCl_2(NCMe)_2$.[31]

Compounds **7** and **8** were determined to be *trans*-$M^{II}(NCS)_2(THF)_4$ (M = V, Ni, respectively). The metal centers are octahedral with four THF molecules in the equatorial planes and two *trans* N-bound thiocyanates (Figure 6). The average M-O bond distances are 2.144(2) Å for **7** and 2.099(1) Å for **8**. The average M-N bond distances are 2.104(3) Å for **7** and 2.005(2) Å for **8**. The ν_{CN} are observed at 2072 and 2127 cm^{-1}, and the δ_{NCS} for M-N are observed at 483 and 471 cm^{-1} for **7** and **8**, respectively, agreeing with terminal *N*-bound thiocyanate ligands. The shortest M···M distances are 7.542 and 7.427 Å for **7** and **8**, respectively.

Compound **9** diffracts strongly; however, the determination of the structure was a challenge because of complex disorder. The hexagonal/trigonal lattice dimensions and extinction symbol (*P*-*c*-) were readily determined, but there are five possible space groups. Elemental analysis, IR, and density measurements lead to a composition of $K_4[V(NCS)_6]\cdot 0.25(OCMe_2)$. Absorptions assignable to terminal, nonbridging ν_{CN} (2115 cm^{-1}), noncoordinated ν_{CO} (1705 cm^{-1}), and δ_{NCS} for M-N (479 cm^{-1}) are present, but a low frequency δ_{NCS} assignable to the M-S absorption is not present. All of this points to the presence of the $[V^{II}(NCS)_6]^{4-}$ ion.

Charge flipping, as implemented in Superflip,[32] provided an electron density map from which it was possible to identify the highest density atomic sites; one of these sites was 6-coordinated and the other appeared to be 2-coordinated. In light of the hypothesized $[V^{II}(NCS)_6]^{4-}$ ion, it was possible to tentatively identify the vanadium and sulfur sites, and populate the model with atoms. This led to decent refinement statistics, but the resulting structure had C−C distances and C−S−C angles impossibly small, and some fractionally occupied sites.

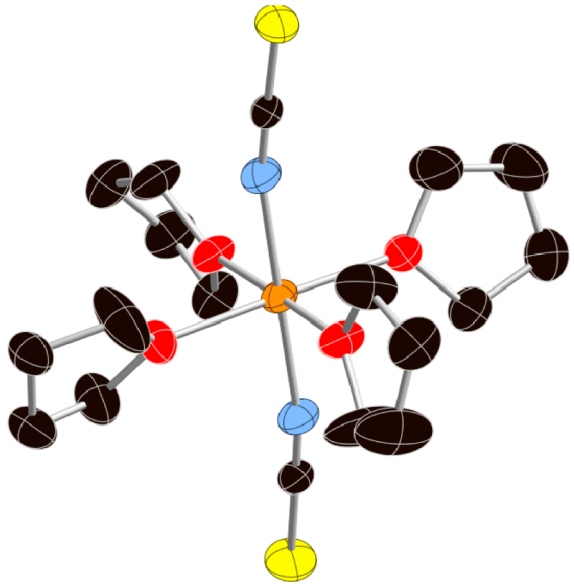

Figure 6. ORTEP drawing (50% probability thermal ellipsoids) structure of *trans*-$V(NCS)_2(THF)_4$ (**7**); orange (V), blue (N), black (C), and yellow (S); hydrogen atoms are omitted for clarity. Compound **8** is isostructural to **7**.

This situation suggests disorder in the structure, but it was difficult to recognize the nature of that disorder in this case. Eventually it was resolved. It is easiest to describe the structure in terms of an ordered model, as shown in Figure 7, with a honeycomb consisting of K^+ ions at the vertices and S atoms on the faces, and the K−S separation is 3.36(1) Å. The $[V(NCS)_6]^{4-}$ ions occupy the channels, fully accounting for all S atoms. Note that if all of the anions in a given channel are shifted by a 6_3 screw axis, they will still bond to the same set of sulfurs.

An ordered version of this structure would have the $P\bar{3}_1m$ space group, but if adjacent channels are disordered, the symmetry is raised to $P6_3/mcm$ with half-occupied V, N, and C sites, and the same cell dimensions. That disorder explains the preliminary refinement observation of half-occupied atom sites and impossibly short interatomic distances. The V−N distance is 2.08(1) Å. The solvent-accessible volume between anions in each

dx.doi.org/10.1021/ic401558f | *Inorg. Chem.* 2013, 52, 10583−10594

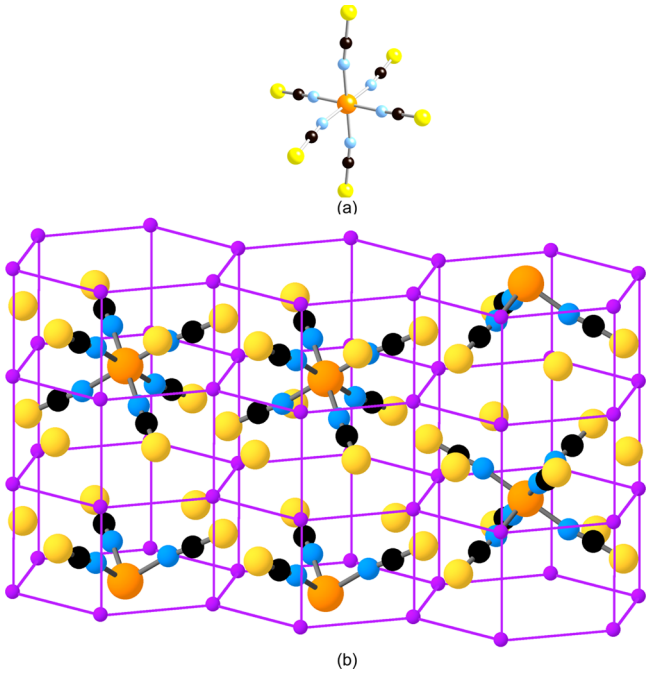

Figure 7. Structure of $[V(NCS)_6]^{4-}$ (a). The ordered parent cell of $K_4[V(NCS)_6]\cdot 0.25(OCMe_2)$ (**9**); orange (V), blue (N), black (C), yellow (S), purple (K). Left and center cells show one placement of the $[V(NCS)_6]^{4-}$ ion along the channels; rightmost cell shows the other placement (b). The acetone solvent in the center of the unit cell is not shown. Isotropic thermal parameters were used, as thermal ellipsoids could not be reliably determined from the available PXRD data. The Ni analogue, **10**, is isostructural to **9**.

chain is 70 Å^3, which would not be enough to accommodate an acetone molecule. Since the ratio of acetone solvent to $[V(NCS)_6]^{4-}$ is 0.25 from the elemental analysis, we infer that there are larger voids, distributed through the lattice, interspersed with $[V(NCS)_6]^{4-}$ units separated by the *c* lattice parameter.

This compound presented a unique crystallographic challenge, inasmuch as the disorder created a situation where the interpretation of the charge map did not lead to a plausible structure. Moreover, it illustrates that atomic positions alone are insufficient to produce a structural model, but rather, a full description must be compatible with known (or hypothesized) chemistry.

Compound **10**, $K_4[Ni(NCS)_6]\cdot 0.25(OCMe_2)$, is isostructural to **9**, and possesses the same disorder. The octahedral Ni^{II} has a Ni–N(CS) bond length of 2.065(6) Å.

Compound **11** was determined to be $Fe(NCS)_2TCNQ$ (Figure 8). The octahedral Fe^{II} centers are bridged by two $\mu_{N,S}$-NCS ligands forming 1-D chains. The 1-D chains are bridged by μ-TCNQ to form 2-D layers. The Fe–N(CS) bond distance is 2.086(11) Å, while the Fe–N(TCNQ) bond distance is 2.212(9) Å, and the Fe–S bond distance is 2.579(3) Å. The Fe···Fe intrachain distance is 5.574 Å and the interchain distance, within the 2-D layer, is 13.413 Å. The shortest Fe···Fe distance between the layers is 6.139 Å. The ν_{CN} absorptions occur at higher frequencies when compared to coordinated $[TCNQ]^{\bullet-}$ (2194, 2134 cm^{-1}), and are comparable to TCNQ^o.[33] The bond distances within the TCNQ could not be determined with sufficient accuracy to ascertain the oxidation state for TCNQ; hence, the infrared and magnetic data are more informative in its assignment.

Magnetic Properties. The temperature dependent magnetic susceptibility, $\chi(T)$, data were taken from 5 to 300 K, and are analyzed as $\chi(T)$, $\chi T(T)$, and $\chi^{-1}(T)$. The 300-K χT value of

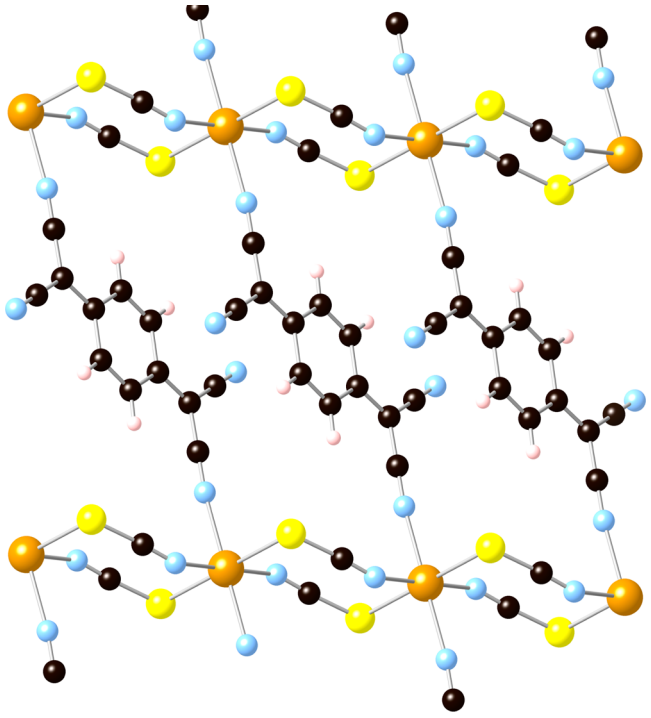

Figure 8. Extended 2-D layer structure of $Fe(NCS)_2TCNQ$ (**11**); gold (Fe), blue (N), black (C), yellow (S), white (H). Isotropic thermal parameters were used, as thermal ellipsoids could not be reliably determined from the available PXRD data.

1 is 3.01 emuK/mol, which correspond to the spin-only values of 3.00 for an $S = 2$ system. The $\chi(T)$ increases as the temperature is decreased, Figure 9. The Curie–Weiss expression, eq 1 with

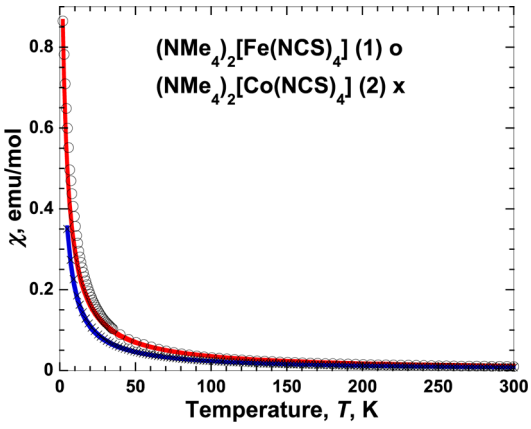

Figure 9. $\chi(T)$ for $(NMe_4)_2[Fe^{II}(NCS)_4]\cdot MeCN$ (**1**) (○) and $(NMe_4)_2[Co^{II}(NCS)_4]$ (**2**) (×) and the Curie–Weiss expression (-) (eq 1) fits with $g = 2$ and $\theta = -1.5$ K for **1** (red line), and $g = 2.25$ and $\theta = -1.7$ K for **2** (blue line).

N = Avogadro's number, μ_B = Bohr Magneton, g = Landé value, k_B = Boltzmann's constant, θ = Weiss constant, and S the total spin quantum number, was used to fit the $\chi(T)$ data with $g = 2.0$ and $\theta = -1.5$ K suggesting antiferromagnetic coupling.

$$\chi = \frac{N\mu_B^2 g^2 S(S+1)}{3k_B(T-\theta)} \quad (1)$$

As **1** possesses a T_d high spin Fe^{II} ion, it should not exhibit significant spin–orbit coupling.[34] However, zero field splitting

dx.doi.org/10.1021/ic401558f | Inorg. Chem. 2013, 52, 10583–10594

(ZFS) should be present; including ZFS, nevertheless, does not improve the fit.

The 300-K χT value of **2** is 2.35 emuK/mol, which is higher than the spin only value of 1.875 emuK/mol for an $S = 3/2$ system. While tetrahedral Co(II) is not as strongly anisotropic as octahedral Co(II), values exceeding the spin-only value are frequently reported.[35a] The $\chi(T)$ increases as the temperature is decreased, Figure 9, and can be fit to the Curie–Weiss expression, $\chi \propto (T - \theta)^{-1}$, eq 1, with $g = 2.25$ and $\theta = -1.7$ K suggesting weak antiferromagnetic coupling, Figure 9.

The room temperature χT value of **3** is 3.16 emuK/mol, corresponding to the spin-only value of 3.00 emuK/mol expected for high spin Fe^{II}. Above 5 K, the data can be fit to the Curie–Weiss expression with $g = 2.09$ and $\theta = -11$ K for **3**, Figure 10. The θ values for **3** suggest antiferromagnetic coupling. The $\chi T(T)$ for **3** has a better fit to an expression that accounts for the zero field splitting (ZFS) present for an $S = 2$ system, eq 2[36] ($H = -2JS_i \cdot S_j$), when compared to the Curie–Weiss expression, as seen in Figure 10. The fitting parameters to eq 2 are $D/k_B = -22$ K, $g = 2.06$, and $\theta = -5$ K.

$$\chi = \left[\frac{1}{3}\frac{N\mu_B^2 g^2 S(S+1)}{3k_B(T-\theta)}\left(\frac{2e^{-D/3k_BT} + 8e^{-4D/3k_BT}}{1 + 2e^{-D/3k_BT} + 2e^{-4D/3k_BT}}\right)\right] + \left[\frac{2}{3}\frac{N\mu_B^2 g^2 S(S+1)}{3k_B(T-\theta)} \times \left(\frac{18 - 14e^{-D/3k_BT} - 4e^{-4D/3k_BT}}{1 + 2e^{-D/3k_BT} + 2e^{-4D/3k_BT}}\right)\right] \quad (2)$$

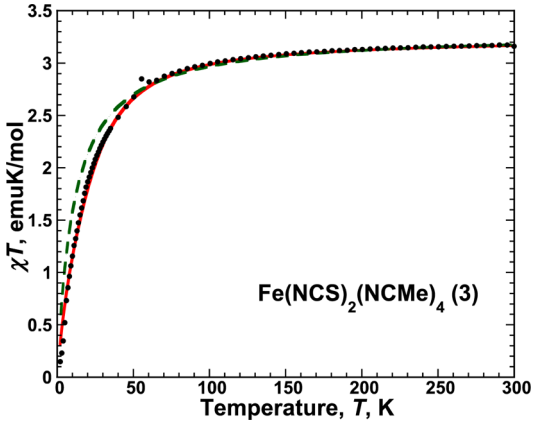

Figure 10. $\chi T(T)$ for **3** (●), and the fits to Curie–Weiss expression, eq 1 (dashed line), and to eq 2 (solid line).

The 300-K χT value of **4** is 1.99 emuK/mol, and this is reduced from the spin-only value of 3.00 emuK/mol for an $S = 2$ system. $\chi(T)$ increases as the temperature is decreased and reaches a maximum of 0.021 emu/mol at 44 K, Figure 11. Below 44 K, $\chi(T)$ decreases until 23 K where the data increases sharply until 5 K. This sharp increase below 23 K is attributed to a small amount of paramagnetic impurities. Above 53 K, $\chi(T)$ could be fit to the Curie–Weiss expression, eq 1, with $g = 2.06$ and $\theta = -90$ K suggesting very strong antiferromagnetic coupling. The cusp-shaped peak in $\chi(T)$ data suggests antiferromagnetic ordering.[37,38] The temperature at which the maximum in $\chi(T)$ occurs exceeds the true T_c[39,40] which is best determined as the

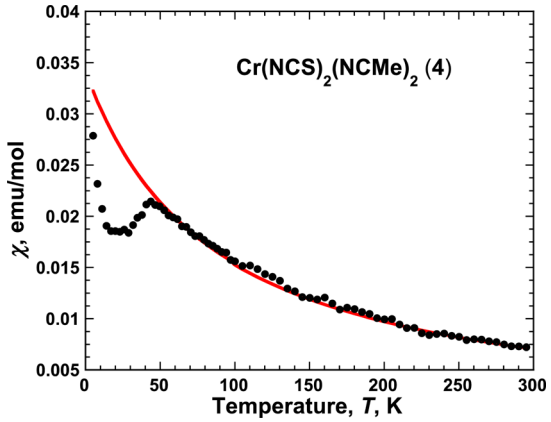

Figure 11. $\chi(T)$ for **4** (●) and the fit to eq 1 (red line) with $g = 2.06$ and $\theta = -90$ K.

temperature at which the maximum in $d(\chi T)/dT$ occurs.[41,42] The $d(\chi T)/dT$ for **4** has a maximum, and thus a T_c of 37 K.

The 300-K χT value of **5** is 3.86 emuK/mol, and it is reduced from the spin-only value 4.375 emuK/mol expected for an $S = 5/2$ system. $\chi(T)$ increases with decreasing temperature and reaches a maximum of 0.051 emu/mol at 22.5 K, Figure 12.

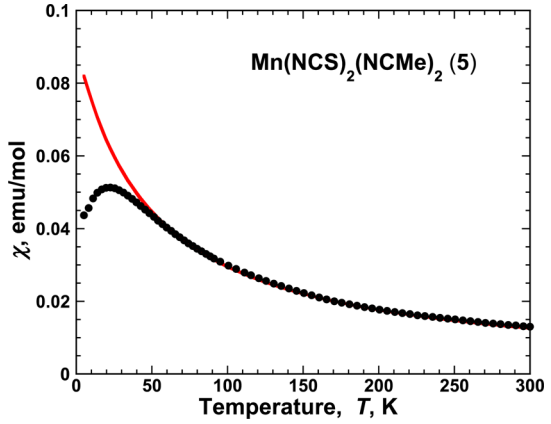

Figure 12. $\chi(T)$ of **5** (●) and the fit to eq 1 with $g = 2.00$ and $\theta = -48$ K.

Likewise, $\chi T(T)$ reaches a maximum at 22.5 K. Below 22.5 K, $\chi(T)$ decreases until 5 K. While the peak in $\chi(T)$ suggests antiferromagnetic ordering with a T_c of 22.5 K, neither a cusp in $\chi(T)$ nor a maximum in the Fisher specific heat, $d(\chi T)/dT$, is evident; hence, ordering does not occur. Thus, above 57 K, $\chi T(T)$ can be fit to the Curie–Weiss expression, eq 1, with $g = 2.00$ and $\theta = -48$ K indicating very strong antiferromagnetic coupling.

The 300-K χT value of **6** is 3.09 emuK/mol and exceeds the spin-only value 1.875 emuK/mol for an $S = 3/2$ system. $\chi(T)$ increases as the temperature is decreased, Figure 13. The $\chi(T)$ and $\chi T(T)$ data can be fit to both eq 1, and the Fisher expression[43] (eq 3; $H = -2JS_i \cdot S_j$) above ~75 K with $g = 2.4$ and $\theta = 4.0$ K, and for eq 3 above ~35 with $g = 2.4$ and $J/k_B = 0.68$ K (0.47 cm^{-1}). The positive J suggests ferromagnetic coupling between the cobalt centers within the chain.

$$\chi = \frac{Ng^2\mu_B^2 S(S+1)}{3k_BT} \times \frac{1+u}{1-u} \quad \text{where} \quad u = \coth\frac{2J(S(S+1)}{k_BT} - \frac{k_BT}{2J(S(S+1)} \quad (3)$$

dx.doi.org/10.1021/ic401558f | Inorg. Chem. 2013, 52, 10583–10594

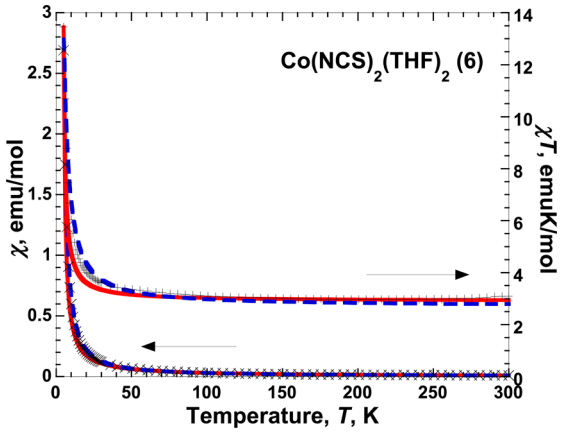

Figure 13. $\chi(T)$ (×) and $\chi T(T)$ (+) for **6** and the fits to eq 1 (red continuous line) with g = 2.4 and θ = 4 K, and the Fisher expression (eq 3) (blue dashed line) with g = 2.4 and J/k_B = 0.68 K (0.47 cm^{-1}).

Compounds **7** and **8** are isostructural to each other and have similar magnetic properties. The 300-K χT values for **7** and **8** are 1.84 and 1.22 emuK/mol, respectively, which correspond to the spin-only values of 1.875 and 1.00 for S = 3/2 and S = 1 systems, respectively. $\chi(T)$ increase as the temperature is decreased, Figure 14. The data was fit to eq 1 for **7** (g = 1.97 and θ = −0.6 K),

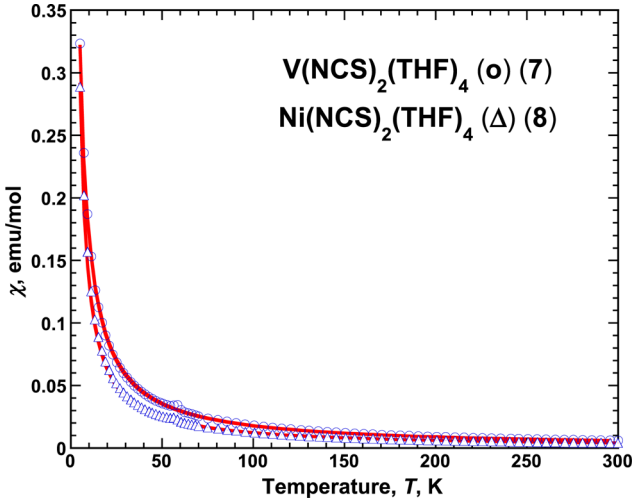

Figure 14. $\chi(T)$ data of **7** (○) and fit to eq 1 (line) with g = 1.97 and θ = −0.6 K, and the $\chi(T)$ data of **8** (Δ) and the fit to eq 1 (line) with g = 2.21 and θ = 0.9 K.

and **8** (g = 2.21 and θ = 0.9 K). The θ-values suggest small antiferromagnetic coupling for **7** and ferromagnetic coupling for **8**.

Compounds **9** and **10** are isostructural to each other and have similar magnetic properties. The 300-K χT values for **9** and **10** are 1.74 and 1.01 emuK/mol, respectively, which correspond to the spin-only values of 1.875 and 1.00 emuK/mol for S = 3/2 and S = 1 systems, respectively. The room temperature values of χT for **9** agree with 1.83 and 1.85 emuK/mol reported for $K_4[V(NCS)_6]\cdot EtOH$[18] and $A_4[V(NCS)_6]$ (A = NMe_4^+, NEt_4^+),[19] respectively. While for **10**, the room temperature value is less than the 1.32 emuK/mol reported for $(NEt_4)_4[Ni(NCS)_6]\cdot EtOH$.[21] The $\chi(T)$ for **9** and **10** increases as the temperature is decreased, Figure 15. The data was fit to the eq 1 for **9** with g = 1.94 and θ = −1.1 K, and for **10** with g = 2.0 and

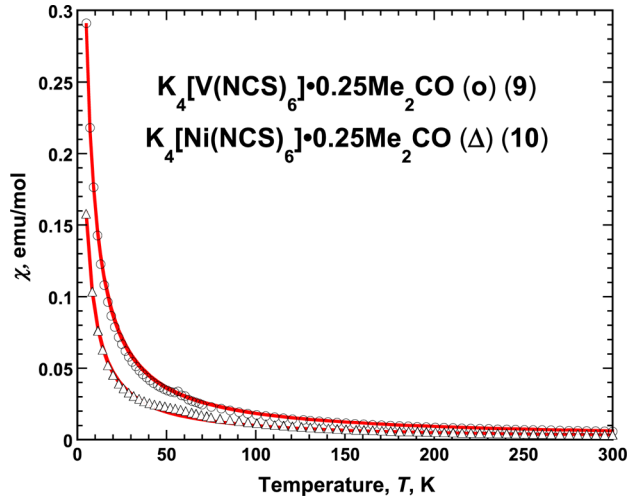

Figure 15. $\chi(T)$ for **9** (○) and the fit to eq 1 (line) with g = 1.94 and θ = −1.1 K, and $\chi(T)$ for **10** (Δ) and the fit to eq 1 (line) with g = 2.0 and θ = −1.3 K.

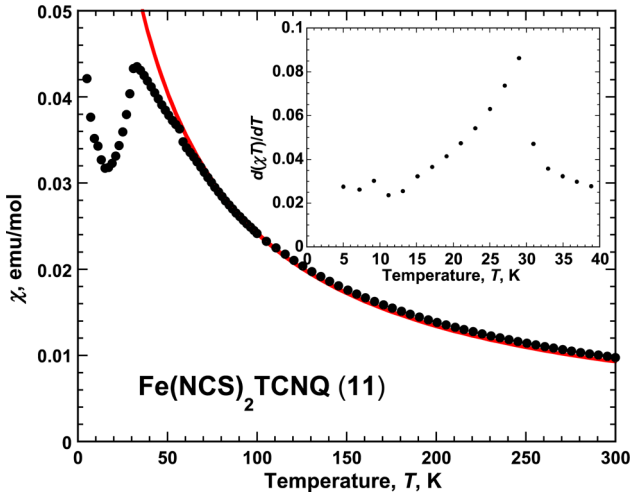

Figure 16. $\chi(T)$ for **11** (○) and the fit to eq 1 (line) with g = 2.0 and θ = −24 K. Inset d(χT)/dT vs T.

θ = −1.3 K. The θ-values suggest small antiferromagnetic coupling for both compounds. The low g-value is in accord with observed values of χT that are reduced spin-only values for other V(II) compounds,[18,35b,44] and low g value of 1.96 for V(II) ions in $CsCaCl_3$.[45] Ferromagnetic impurities (48 ppm Fe) were used to correct the upturn of the $\chi T(T)$ data for **9**.

Compounds **7**−**10** have isolated metal ion coordination centers and have weak, through space interactions. These isolated species typically exhibit weak antiferromagnetic coupling, but in some cases ferromagnetic coupling is observed. There is not, unfortunately, an understanding as to why some compounds couple ferromagnetically.

The 300-K χT value of **11** is 2.93 emuK/mol, close to the spin-only value 3.00 emuK/mol for an S = 2 system. $\chi(T)$ increases with decreasing temperature, and reaches a maximum of 0.044 emu/mol at 33 K, Figure 16. Below 33 K, $\chi(T)$ decreases until 15 K where the data increases sharply until 5 K. This sharp increase below 15 K is attributed to a small amount of paramagnetic impurities. Above 33 K, the Curie−Weiss expression was used to fit the $\chi(T)$ data with g = 2.0 and θ = −24 K suggesting antiferromagnetic coupling. The peak in the $\chi(T)$ data suggests

dx.doi.org/10.1021/ic401558f | Inorg. Chem. 2013, 52, 10583−10594

antiferromagnetic ordering[37] with a T_c determined from the maximum in $d(\chi T)/dT$[39,40] of 29 K, Figure 16.

CONCLUSION

Several new first row transition metal thiocyanate complexes have been prepared. Reactions of M(II) precursors with thiocyanate in acetonitrile produce 0-D tetrahedral [e.g., $[M(NCS)_4]^{2-}$] and octahedral [e.g., $M(NCS)_2(NCMe)_4$], 1-D [e.g., $Co(NCS)_2(THF)_2$], 2-D [e.g., $Mn(NCS)_2(NCMe)_2$], and 3-D [e.g., $Cr(NCS)_2(NCMe)_2$] structured metal thiocyanate complexes. The isolated tetrahedral and octahedral complexes are paramagnetic. 1-D $Co(NCS)_2(THF)_2$ has *trans*-THFs, and its magnetic behavior can be modeled via an 1-D Fisher expression ($H = -2JS_i \cdot S_j$) with $g = 2.4$ and $J/k_B = 0.68$ K (0.47 cm^{-1}) and exhibits weak ferromagnetic coupling. The 2-D and 3-D $M(NCS)_2(NCMe)_2$ (M = Cr, Mn) have acetonitriles in a *cis* orientation. The 2-D $Mn(NCS)_2(NCMe)_2$ is best described as $Mn_2(\mu_{N,N}\text{-}NCS)_2(\mu_{N,S}\text{-}NCS)_2$ with the latter $\mu_{N,S}$-NCS providing the 2-D connectivity. $Cr(NCS)_2(NCMe)_2$ magnetically order as an antiferromagnet with a T_c of 37 K, while $Mn(NCS)_2(NCMe)_2$ exhibits strong antiferromagnet coupling. In contrast, $Mn(NCS)_2(NCMe)_2$ exhibits antiferromagnetic coupling with $\theta = -48$ K, and $M(NCS)_2(THF)_4$ and $K_4[M(NCS)_6]$ (M = V, Ni) are weakly coupled paramagnets as expected for 0-D metal complexes. The reaction of TCNQ and iron thiocyanate yields a 2-D layer of $Fe^{II}(NCS)_2TCNQ^o$, and is an antiferromagnet with ordering temperature of 29 K.

ASSOCIATED CONTENT

Supporting Information

The observed PXRD as well as Rietveld fits for **2**, **4**, **9**, **10**, and **11**. The X-ray crystallographic CIF files for **1**−**11** (CCDC#806643, 945401, 806646, 945402, 945403, 806644, 806642, 806648, 945404, 945405, and 945406), respectively. This material is available free of charge via the Internet at http://pubs.acs.org

AUTHOR INFORMATION

Corresponding Author

*E-mail: jsmiller@chem.utah.edu.

Present Addresses

[‖]Department of Chemistry and Chemistry Research Center, United States Air Force Academy, Colorado Springs, CO 80840. [⊥]Argonne National Laboratory, Argonne, IL 60439-4856.

Notes

The authors declare no competing financial interest.

ACKNOWLEDGMENTS

We appreciate the helpful discussions with Nhi Ma, and assistance from Joshua E. Sussman, and the late Joshua D. Bell and preliminary work provided by Thomas E. Vos, as well as the continued support by the Department of Energy Division of Material Science (Grants DE-FG03-93ER45504) to E.S. and J.S.M. for the chemical synthesis, chemical, and spectroscopic characterization, and magnetic studies. C.E.M. and A.L.R. executed the single crystal X-ray analyses. Use of the National Synchrotron Light Source, Brookhaven National Laboratory, to execute powder X-ray diffraction studies by S.H.L. and P.W.S. was supported by the U.S. Department of Energy, Office of Basic Energy Sciences, under Contract No. DE-AC02-98CH10886.

REFERENCES

(1) Bailey, R. A.; Kozak, S. L.; Michelsen, T. W.; Mills, W. N. *Coord. Chem. Rev.* **1971**, *6*, 407.

(2) Burmeister, J. L. *Coord. Chem. Rev.* **1990**, *105*, 77.

(3) (a) Defotis, G. C.; Barlowe, C. K.; Shangraw, W. R. *J. Magn. Magn. Mater.* **1986**, *54*, 1493. (b) Dockum, B. W.; Reiff, W. M. *Inorg. Chem.* **1982**, *21*, 391. (c) Flint, C. D.; Goodgame, M. *J. Chem. Soc. A* **1970**, 442. (d) Nather, C.; Greve, J. *J. Solid State Chem.* **2003**, *176*, 259. (e) McElearney, J. N.; Balagot, L. L. *Phys. Rev. B* **1979**, *19*, 306.

(4) Shurdha, E.; Lapidus, S. H.; Stephens, P. W.; Moore, C. E.; Rheingold, A. R.; Miller, J. S. *Inorg. Chem.* **2012**, *51*, 9655.

(5) Oki, H.; Kyuno, E.; Tsuchiya. *Bull. Chem. Soc. Jpn.* **1968**, *41*, 2357.

(6) Kranz, M. *Inorg. Syn.* **1963**, *7*, 94.

(7) Buschmann, W. E.; Miller, J. S. *Chem.—Eur. J.* **1998**, *4*, 1731.

(8) Rosenheim, A.; Cohn, R. *Z. Anorg. Chem.* **1901**, *27*, 289.

(9) Brandon, E. J.; Rittenberg, D. K.; Arif, A. M.; Miller, J. S. *Inorg. Chem.* **1998**, *37*, 3376.

(10) (a) *Handbook of Chemistry and Physics*, 64th ed.; Weast, R. C., Ed.; CRC Press: Boca Raton, FL, 1984; pp 109−125. (b) Bain, G. A.; Berry, J. F. *J. Chem. Educ.* **2008**, *85*, 532.

(11) (a) *Saint Plus*, v. 6.02; Bruker Analytical X-ray: Madison, WI, 1999. (b) Sheldrick, G. M. *SADABS*; University of Göttingen: Göttingen, Germany, 1996.

(12) (a) Goldberg, I.; Krupitsky, H.; Stein, Z.; Hsiou, Y.; Strouse, C. E. *Supramol. Chem.* **1995**, *4*, 203. (b) Krupitsky, H.; Stein, Z.; Goldberg, I. *J. Inclusion Phenom. Mol. Recognit. Chem.* **1995**, *20*, 211. (c) Goldberg, I. *Mol. Cryst. Liq. Cryst.* **1996**, *278*, 767. (d) Byrn, M. P.; Curtis, C. J.; Hsiou, Y.; Khan, S. I.; Sawin, P. A.; Tendick, S. K.; Terzis, A.; Strouse, C. E. *J. Am. Chem. Soc.* **1993**, *115*, 9480. Byrn, M. P.; Curtis, C. J.; Hsiou, Y.; Khan, S. I.; Sawin, P. A.; Terzis, A.; Strouse, C. E. In *Comprehensive Supramolecular Chemistry*; Atwood, J. L., Davies, J. E. D., MacNicol, D. D., Vogtle, F., Eds.; Pergamon: New York, **1996**; Vol. *6*, p 715.

(13) *TOPAS V4.1: General profile and structure analysis software for powder diffraction data*, User's Manual; Bruker AXS: Karlsruhe, Germany, 2005.

(14) Coelho, A. A. *J. Appl. Crystallogr.* **2000**, *33*, 899.

(15) *TOPAS-Academic*, v4.1 available at www.topas-academic.net.

(16) Forster, D.; Goodgame, D. M. L. *J. Chem. Soc.* **1965**, 268.

(17) Lewis, J.; Nyholm, R. S.; Smith, P. W. *J. Chem. Soc.* **1961**, 4590.

(18) Trageser, G.; Eysel, H. H. *Inorg. Chem.* **1977**, *16*, 713.

(19) Larkworthy, L. F.; Tucker, B. J. *J. Chem. Soc., Dalton Trans.* **1980**, 2042.

(20) Nakamoto, K. *Infrared and Raman Spectra of Inorganic and Coordination Compounds*; Part B: Applications in Coordination, Organometallic, and Bioinorganic Chemistry, 5th ed.; Wiley-Interscience: New York, 1997; p 111.

(21) Forster, D.; Goodgame, D. M. L. *Inorg. Chem.* **1965**, *4*, 823.

(22) Handa, M.; Yoshioka, D.; Sayama, Y.; Shiomi, K.; Mikuriya, M.; Hiromitsu, I.; Kasuga, K. *Chem. Lett.* **1999**, 1033.

(23) Ghazzali, M.; Langer, V.; Öhrström, L. *J. Solid State Chem.* **2008**, *181*, 2191.

(24) Akers, C.; Peterson, S. W.; Willett, R. D. *Acta Crystallogr., Sect. B* **1668**, *24*, 1125.

(25) Crystal structure illustrations prepared with CrystalMaker; www.crystalmaker.com

(26) Buschmann, W. E.; Miller, J. S. *Chem.—Eur. J.* **1998**, *4*, 1731.

(27) Filatkina, B. C. *Zh. Strukt. Khim.* **1969**, *10*, 274.

(28) McElearly, J. N.; Balagot, L. L.; Muir, J. A.; Spence, R. D. *Phys. Rev. B* **1979**, *19*, 307.

(29) Boeckmann, J.; Näther, C. *Polyhedron* **2012**, *31*, 587. Boeckmann, J.; Näther, C. *Dalton Trans.* **2010**, *39*, 11019.

(30) Richards, P. M.; Quinn, R. K.; Morosin, B. *J. Chem. Phys.* **1973**, *59*, 4474. Clark, R. J. H.; Williams, C. S. *Inorg. Chem* **1965**, *4*, 350. Dunitz, J. D. *Acta Crystallogr.* **1957**, *10*, 307. Goodgame, D. M. L.; Goodgame, M.; Hitchman, M. A.; Weeks, M. J. *Inorg. Chem.* **1966**, *5*, 635. Long, G. J.; Whitney, D. L.; Kennedy, J. E. *Inorg. Chem.* **1971**, *10*, 1406. Zurowska, B.; Mrozinski, J.; Julve, M.; Lloret, F.; Maslejova, A.; Sawka-Dobrowolska, W. *Inorg. Chem.* **2002**, *41*, 1771.

(31) Pokhodnya, K. I.; Bonner, M.; DiPasquale, A. G.; Rheingold, A. L.; Her, J.-H.; Stephens, P. W.; Park, J.-W.; Kennon, B. S.; Arif, A. M.; Miller, J. S. *Inorg. Chem.* **2007**, *46*, 2471.
(32) Palatinus, L.; Chapuis, G. *J. Appl. Crystallogr.* **2007**, *40*, 786.
(33) Motokawa, N.; Oyama, T.; Matsunaga, S.; Miyasaka, H.; Yamashita, M.; Dunbar, K. R. *CrystEngComm* **2009**, *11*, 2121.
(34) Colignon, D.; Kartheuser, E.; Rodriguez, S.; Villeret, M. *Phys. Rev. B* **1995**, *51*, 4849.
(35) (a) Boudreaux, E. A.; Mulay, L. N. *Theory and Applications of Molecular Paramagnetism*; Wiley-Interscience: New York, 1976; p 218. (b) p 159.
(36) O'Connor, C. J. *Prog. Inorg. Chem.* **1982**, *29*, 203.
(37) Carlin, R. L. *Magnetochemistry*; Springer-Verlag: Berlin, Germany, 1986; p 121.
(38) Morrish, A. H. *The Principles of Magnetism*; Krieger Publishing Co., Inc.: Huntington, NY, 1980; p 490ff.
(39) Fisher, M. E. *Philos. Mag.* **1962**, *7*, 1731.
(40) Ashcroft, N. W.; Mermin, N. D. *Solid State Physics*; W. B. Saunders and Co.: Philadelphia, PA, 1976; p 701 ff.
(41) Aharen, T.; Greedan, J. E.; Ning, F.; Imai, T.; Michaelis, V.; Zhou, H.; Wiebe, C. R.; Cranswick, L. M. D. *Phys. Rev. B* **2009**, *80*, 134423.
(42) Cage, B.; Nguyen, B.; Dalal, N. *Solid State Commun.* **2001**, *119*, 597.
(43) Kahn, O. *Molecular Magnetism*; VCH: New York, 1994; p 258.
(44) Figgis, B. N.; Lewis, J.; Mabbs, F. *J. Chem. Soc.* **1960**, 2480.
(45) McPherson, G. L.; Freedman, M. R. *Inorg. Chem.* **1976**, *15*, 2299.